12-16-1987

Industrial Applications of Auger Surface Analysis

R. E. Chase
Ford Motor Company Scientific Research Laboratories

G. S. Cole
Ford Motor Company Scientific Research Laboratories

Recommended Citation

Utah State University
MERRILL-CAZIER LIBRARY

INDUSTRIAL APPLICATIONS OF AUGER SURFACE ANALYSIS

R. E. Chase* and G. S. Cole

Ford Motor Company
Scientific Research Laboratories

Abstract

Scanning Auger microscopy is distinguished by its unique combination of surface selectivity, high spatial resolution, ease of identifying elements and quantifying composition, and ability to distinguish between chemical states.

This paper describes several applications of scanning Auger microscopy, emphasizing the range of industrial research activities:

1. Electronic Materials. Contamination in an integrated circuit processing facility was identified and procedures for its removal determined. Causes for the delamination of printed circuit board foils were identified. Superlattice films were characterized and the deposition process evaluated.

2. Tribology. Analysis of surfaces in lubricated sliding contact revealed the effects of contact kinematics and of molybdenum anti-friction additives.

3. Corrosion. Early growth stages of phosphate coatings were found to be associated with a thin phosphate layer, not visible in SEM, interspersed with larger crystals. A corrosion layer on stainless steel/aluminum bimetal trim was shown to contain calcium carbonate and silicate deposits consistent with its galvanic protection mechanism.

4. Catalysis. Oxidation studies of Pd/Rh alloys revealed varying surface compositions as a function of heat treatment temperature.

Several problems commonly encountered in Auger analysis are described and ways of minimizing or estimating their effects are discussed.

*Address for correspondence:
Ford Motor Company
SRL Room S-1022
PO Box 2053
Dearborn, MI 48121   Phone No. (313) 594-7292

Introduction

Auger electron spectroscopy is one of the most widely used of the surface analytical tools and has been the subject of many reviews. A few of the more recent books are listed in the references (Feldman and Mayer, 1986; Thompson et al., 1985; Briggs and Seah, 1983; Casper and Powell, 1982). It is not the purpose of this article to give another general review, but rather to discuss methods of approach and problems encountered in several applications that are typical of an industrial research laboratory.

Scanning Auger microscopy provides elemental analysis of the near surface region of a sample, as well as depth profiles showing how elements are distributed below the surface. In addition, newer instruments can provide high magnification images of the surface so that composition can be related to topography. In failure analysis work, a modern Auger instrument can locate and identify the contaminants which cause failure. In tribology, corrosion, and conversion coatings studies, such features as wear debris, small crystals, pores and nucleating particles have micron to submicron dimensions which are accessible in such an instrument. Modern scanning Auger instruments have spatial resolution approaching that of a scanning electron microscope (SEM). They can thus positively correlate chemical analyses with surface details.

While high spatial resolution is a very desirable feature, much useful information can be obtained with older instruments. Such instruments retain the advantages of Auger analysis, which include excellent depth resolution, ease of identifying elements, ability to yield quantitative compositions, high sensitivity to the light elements, and ability to distinguish between chemical states for selected elements. Some of the limitations of poor spatial resolution can be overcome by combining Auger analysis with subsequent SEM studies to characterize the surface topography. The applications discussed here were approached in such a manner.

The examples we have selected demonstrate the flexibility of scanning Auger in solving industrial problems. They were chosen because they show how complex such problems can be.

The research areas which use scanning Auger analysis at our facility reflect the increasing emphasis on surfaces brought about by such issues as increased product reliability and quality, and application of high technology to the automotive industry.

Materials and Methods

The data were obtained using a Perkin Elmer PHI Model 545 scanning Auger microprobe. The instrument was run either with a focused beam (to about 5 μm) during imaging or with the beam defocused to a diameter of 240 μm for most acquisitions of Auger spectra. Beam currents ranged from 0.1 to 1 μA (corresponding to current densities of 0.3 to 3 mA/cm^2) for a primary electron beam of 3 or 5 keV. Auger spectra were acquired in the derivative mode with a modulation amplitude of 3 eV and were converted to semiquantitative compositions using peak-to-peak heights and employing, in most cases, sensitivity factors derived from handbook spectra (Davis et al., 1976).

Sputter depth profiling is an important part of the scanning Auger method. During profiling, Auger spectra were usually taken at a vacuum of 5 x 10^{-5} Torr, alternating with periods of sputtering by a rastered 2 keV argon ion beam. The ion gun conditions were chosen to give a removal rate of 0.01 nm/sec from a Ta$_2$O$_5$ standard. These relatively gentle sputtering conditions allowed detailed profiles of thin surface layers and minimized sputtering artifacts.

Most specimens were mounted as received. In those cases where contamination from handling and/or environment was expected to adversely affect vacuum integrity, samples were rinsed in ethanol. When samples required cutting, it was done dry with a clean jeweler's saw or with a diamond wheel in a clean, dedicated saw using isopropanol as a cutting fluid. In the examples that follow, deviations from these procedures are noted as they apply.

Results and Discussion

Electronic Materials Applications

Scanning Auger microscopy has many applications in the development and fabrication of semiconductor devices, including integrated circuits. At Ford's Scientific Research Laboratories we have used the technique to investigate metallization, interdiffusion, protective barrier layers, and oxide growth characteristics. Why and how devices or circuits failed (i.e., general failure analysis) is also an important use of scanning Auger microscopy.

IC Fabrication/Contamination. Scanning Auger microscopy was successfully employed to identify and allow elimination of contaminants in critical components during the construction of a clean room facility at Ford Research. The suspect components were sections of stainless steel tubing being installed to distribute high purity gases to the oxidation and diffusion furnaces. By sampling various locations on the interior of the tubing, we were able to identify

one set of contaminants as residues from the cleaning procedures used by the tubing supplier. Sodium, chlorine, phosphorus, calcium, and carbon were detected in a layer of contaminant on the surface estimated to be 10-20 nm thick. A detailed analysis of the phosphorus Auger line shape indicated that the phosphorus was present as a phosphate, probably from trisodium phosphate used in cleaning. Previous work in this laboratory (Willermet et al., 1983) had shown that phosphorus as phosphate was distinguished by the presence of peaks at 86, 94, and 106 eV, instead of the single peak at 120 eV for phosphide. To reproducibly detect phosphate and avoid reducing it to phosphide, the electron beam current density had to be kept low, at about 0.3 mA/cm^2 (corresponding to a beam current of 100 nA and beam diameter of about 240 μm).

In a second tube, detailed examination of the oxygen Auger line showed that the largely carbonaceous residue came from a different source, most likely an oil.

We verified the effectiveness of simple rinsing in hot deionized water to remove the sodium, chlorine, phosphate, and calcium. Our recommendation of a bakeout under vacuum was shown to remove the remaining contaminants, resulting in sufficient cleanliness for subsequent uncontaminated operation of the oxidation and diffusion furnaces.

Printed Circuit Boards. Printed circuit boards are usually composed of a conductive, copper-base foil (approximately 30-50 μm thick) bonded to a polymer substrate. The electrical circuitry is obtained using a process of conventional photolithography followed by chemical dissolution or etching of the foil into approximately 300 μm wide, wire-like conductive paths or "lines". Assembly is completed by inserting the appropriate circuit components and using wave soldering to make the electrical connections.

We recently examined a series of boards where the etched lines had lifted from the polymer. The boards in question consisted of fiberglass-filled epoxy (rated as NEMA FR4 grade) with a 1 oz. copper foil (35 μm thick). The foil had a final layer of brass on the substrate side to improve long term adhesion. This configuration is quite common in the industry (Bucci, 1984). The unique feature of these boards was the manner in which the brass layer was created -- first by depositing a layer of zinc and relying on curing temperatures (about 190 C) to interdiffuse and alloy the zinc with the copper. The zinc layer was protected from staining (growth of oxide) prior to attachment to the glass/epoxy "prepreg" by a chromate conversion layer.

Examination of the failed boards showed that complete liftoff of the foil was rare; more often, lines were lifted at their edges while still adhering at their centers. Lines of foil were physically removed from the board with scalpel and tweezers for examination and analysis. Although the board surface beneath the removed foil was not analyzed, examination in the optical microscope gave no evidence of metal

still remaining. Optical microscopy of the foils showed a reddish band, about 25-75 μm wide at each edge of lifted lines. Scanning Auger microscopy verified that this region had a higher copper and lower zinc concentration than the brass-colored central region. Auger line scans for a typical foil are given in Figure 1 and show a much higher copper signal in the edge region. From this and evidence presented below, we concluded that the problem was caused by etchant undercutting the foil, dissolving away some of the material at the edges, and reducing the foil's adhesion to the epoxy.

Given that the etchant was cupric chloride, the presence of chlorine at the foil edge and its absence in the center (Figure 2) was consistent with the interpretation that the edge was attacked by the etchant. While carbon was seen everywhere on the surface, it was higher in the central, unattacked region. This could be expected, since some of the epoxy would remain attached to the foil in the region of good adhesion. Where it was bad, due to the undercutting, there would be less epoxy adhering, as observed.

Figure 3 shows the result of sputtering through the edge and central regions of a lifted-off foil line. Six elements are shown plotted: Zn, Cu, Cr, O, C and Cl. The profile was obtained while sputtering for a total of 5000 seconds (corresponding to profiling through 50 nm of a Ta_2O_5 standard); results for the first 1500 seconds are shown here. Figure 3a is representative of the edge (attacked region) at the foil/polymer interface. The elements Zn and O are present and there is a measurable concentration (20%) of Cu in the first 200 seconds. The Cr and part of the O signal represent residues of the chromate coating mentioned above. The C level reduces to zero after 1000 seconds (approximately 10 nm), while the Cl concentration stays nearly constant.

The chemistry in the central, or unattacked region, is different: the Cu concentration is essentially zero at the surface, and the Zn and O levels are higher than at the edge, persisting for 300 seconds of sputtering. The Cl content at the surface is at ambient contamination levels commonly seen on many samples; below the surface the Cl level decreases to zero immediately. Although the C signal decreases, it does not disappear. The C and Cl concentrations are interpreted as previously discussed.

The relationship among the Zn, O and Cu contents is more difficult to understand. There is Zn at the surface in a nonmetallic form, probably as a Zn chromate or oxide (or a mixture of the two), judging from the presence of oxygen and the lower energy of the LMM line. (The MVV line might be expected to be more sensitive to chemical state, but there is an interference of MVV lines for copper and zinc in most spectra.) The oxygen concentration decreases quite rapidly as the surface is sputtered away. The energy of the LMM Zn transition increases and approaches that for metallic Zn. Note that the chromium and oxygen remain for relatively long sputtering times, partly due to the roughness of the surface and the consequent lowered sputter rate for
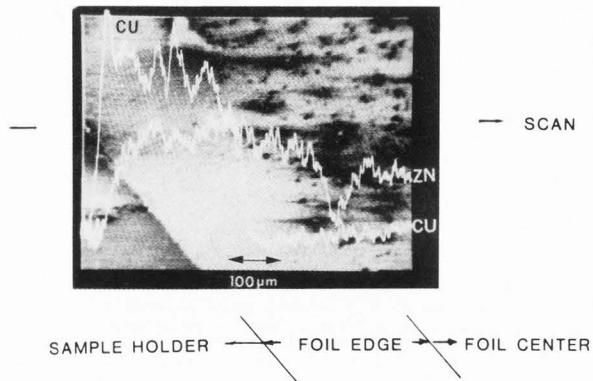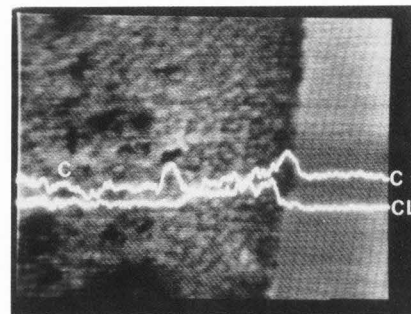

SAMPLE HOLDER — FOIL EDGE — FOIL CENTER

Figure 1. Auger line scans for Cu and Zn superposed on an SEM image of a typical lifted printed circuit foil. Note the region of higher Cu at the foil edge that suffered etchant attack.

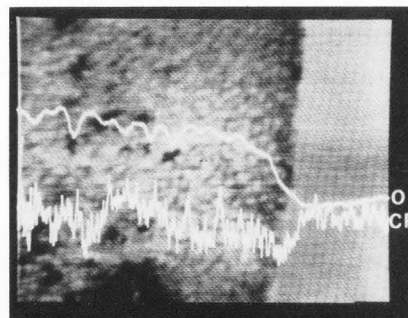| FOIL CENTER | FOIL EDGE | SAMPLE HOLDER |

Figure 2. Auger line scans for C, Cl and Cr, superposed on the SEM image of a typical lifted printed circuit foil.

"shadowed" areas. The absence of a copper signal before sputtering implies a fairly thick layer of zinc oxide/chromate on the surface. From the expected escape depth of about 3 nm for the Cu
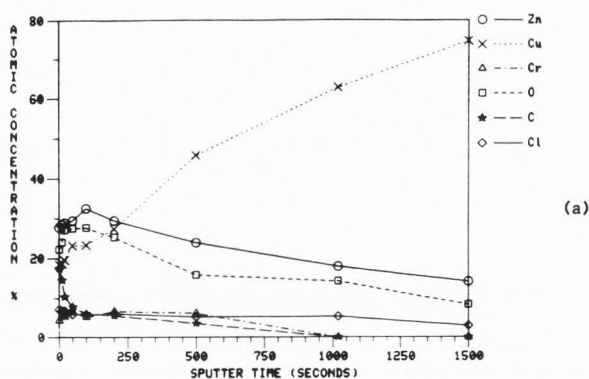
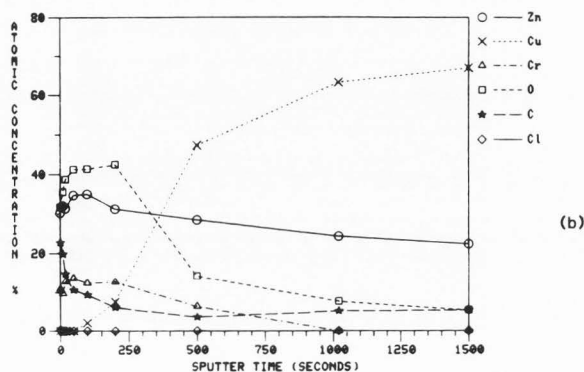Figure 3a. Depth profile of edge region of lifted printed circuit foil.

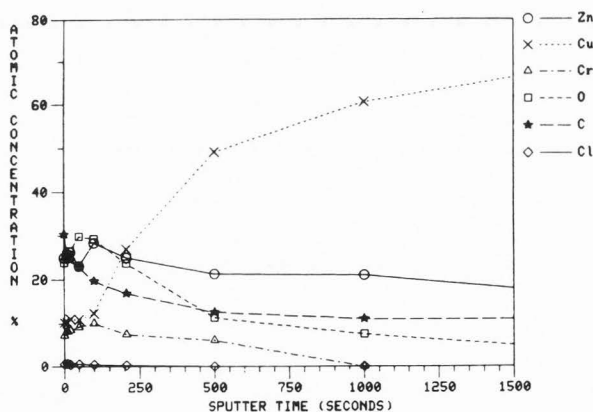Figure 3b. Depth profile of center region of lifted printed circuit foil.

Figure 4. Depth profile of center region of printed circuit foil made by another process; compare with Figure 3b.

LMM Auger electrons (Seah and Dench, 1979), its thickness can be estimated as several tens of nanometers.

The foil delamination was concluded to result from the process used to create the brass layer -- the separate deposition of zinc onto the copper and subsequent processing steps. While the alloying step itself did not appear to cause the problem, the existence of an unalloyed zinc layer may have contributed. Apparently, the processing allowed formation of an excessive thickness of zinc oxide and/or chromate which was susceptible to attack and then undercutting by the etchant. For example, acidic chloride solutions are known to attack zinc oxide much more rapidly than they do brass (van Ooij, 1977). Because of the narrow crevice formed, rinsing did not remove all the etchant, possibly allowing continued attack. The presence of the copper signal before sputtering in the edge region (Figures 1 and 3a) and its absence in the center region (Figures 1 and 3b) show that the zinc oxide/chromate layer has been at least partially removed near the edge.

Copper foil prepared by other procedures, such as by direct electrodeposition of brass onto copper, did not show any "lift-off" and did not show any of the surface changes noted above. There are no differences between the edges and center of the etched lines removed from the boards. Figure 4 shows a typical depth profile. In contrast to Figure 3b, copper is seen before sputtering begins, implying a relatively thin layer of zinc chromate on the surface.

Superlattice of IV-VI Compound Semiconductors. Work on thin films of IV-VI compound semiconductors for application as infrared radiation detectors has been pursued at Ford for several years (Holloway, 1980). Some time ago, studies were begun of PbTe-SnTe superlattices deposited epitaxially on barium fluoride. Samples were analyzed by Auger electron spectroscopy and depth profiled by sputtering to characterize the films and the growth process. Results from one of the early films illustrate some of the problems that can arise in interpreting depth profiles, including estimating the sputter rate, ion beam effects (such as preferential sputtering and mixing), and analysis depth effects.

Auger spectra were acquired using a 3 keV, 200 nA electron beam focused to a diameter of about 240 μm. Depth profiles were obtained by alternating the sputtering with acquisition of Auger spectra. Figure 5 plots the calculated atomic concentrations for lead, tin, tellurium, oxygen, and carbon versus sputter time. The Pb and Sn concentrations are clearly seen to vary periodically, 180 degrees out of phase with each other. In addition, the Te profile is nearly constant in the interior of the film with a concentration of about 50%, as expected. Two unusual features are (1) the disruption of the periodicity at the surface, including the presence of oxygen and (2) the shape of the Pb and Sn profiles in the interior of the film, which ideally should be square waves that stretch from 0 to 50% atomic concentration.

The surface disruption is apparently a result of oxidation. Oxygen is found only in the

near-surface region. The increased Sn concentration in the same region suggests that oxygen is largely present as tin oxide, most likely formed when the sample was exposed to air after deposition. The lower Pb and Te contents near the surface suggest segregation of Sn to the oxide layer.

In order to understand the reason for the rounded and vertically displaced profiles for Pb and Sn, it is helpful to have an estimate for the layer spacing, which can be found from the sputter rate. The profile was obtained with a rastered 2 keV argon ion beam under conditions that gave a sputter rate of 0.01 nm/second on a Ta_2O_5 standard. It is common practice to assume that the sputter rate for the sample of interest is not too different from that for Ta_2O_5. In our case, that assumption is far from correct. As we will see, the rate for PbTe is about 10 times that of Ta_2O_5.

Because we were unable to obtain a standard of known thickness and composition for PbTe or SnTe, we used the following procedure to calculate the sputter rate from tabulated sputter yields. The basic relationship between sputter rate and sputter yield for a single element (or molecule) is given by:

$$r = 100 \, (1/N_A) \, (M/d) \, (J/q_e) \, Y, \qquad (1)$$

where
r = sputter rate (nm/sec),
$N_A = 6.02 \times 10^{23}$ molecules/mole,
M = gram atomic (or molecular) weight,
d = density (g/cm³),
J = effective current density of ion beam (μA/cm²),
$q_e = 1.6 \times 10^{-19}$ Coulombs,
Y = sputter yield (atoms or molecules/ion).
(The factor of 100 is for units conversion.)

The value of J for the sputter conditions we used is obtained from our sputter rate calibration of Ta_2O_5. Using 0.01 nm/second for r and a literature value of 0.3 for Y (Bevolo, 1981), we get $J = 6 \, \mu$A/cm², the effective ion beam current density to be used in the above expression to convert tabulated yields into sputter rates appropriate to our conditions.

For compounds where the sputter yield, Y, has not been measured, an expression analogous to equation (1) but involving elemental sputter yields can be derived, assuming equilibrium has been reached (that is, each element is being sputtered at a rate proportional to the bulk composition). For the case of $Pb_xSn_{(1-x)}Te$, the expression is:

$$r = \frac{100(1/N_A)(M_x/d_x)(J/q_e)}{[1/Y_{Te} + x/Y_{Pb} + (1-x)/Y_{Sn}]} \qquad (2)$$

where
$M_x = 334.8 - 88.5 \, x$,
$d_x = 8.16 - 1.68 \, x$.
Here the additional assumption must be made that the individual sputter yields are the same as those for the pure elements, because data for the matrix $Pb_xSn_{(1-x)}Te$ are not available. This additional assumption is probably the largest source of error in the estimate, as matrix effects are known to alter sputter yields.

Table 1 summarizes the results for several elements and compounds of interest, calculated using equations (1) and (2). Note in particular that the sputter rates for Pb and Te are nearly 10 times that for tantalum oxide and the rate for Sn is almost 5 times that for tantalum oxide. The results for various (Pb,Sn)Te compounds range from 0.07 to 0.10 nm/sec. That means that the 130 seconds of sputter time for one superlattice period (comprising one PbTe layer plus one SnTe layer) corresponds to 9 to 13 nm thickness. This range brackets the expected value of 11 nm obtained from independent interferometric measurements of the total film thickness. The good agreement is somewhat fortuitous, given the assumptions made in the calculation. But it dramatically points out the desirability of making the calculation whenever feasible instead of taking the sputter rate of tantalum oxide as a good estimate.

TABLE 1. SPUTTER RATES FOR SEVERAL ELEMENTS AND COMPOUNDS OF INTEREST

Element or Compound	Gram Molecular Weight (grams)	Density (g/cm³)	Sputter[a] Yield	Sputter Rate (nm/sec)
Ta_2O_5	441.8	8.2	0.3[b]	0.010[e]
Ta	181.0	16.6	2.1[c]	0.014[f]
Cu	63.5	8.9	3.2[c]	0.014[f]
Sn	118.7	7.2	4.5[c]	0.046[f]
Te	127.6	6.2	7.4[c]	0.095[f]
Pb	207.2	11.3	8.2[c]	0.094[f]
PbTe	334.8	8.16[d]	---	0.099[g]
SnTe	246.3	6.48[d]	---	0.066[g]

Notes: [a]Sputter yield for argon at 2 keV

[b](Bevolo, 1981)

[c]Extrapolated values for 2 keV from data for 1 keV and under (Seah, 1981)

[d](Gray, 1972)

[e]Measured rate for experimental conditions

[f]Rates calculated from equation (1) for experimental conditions

[g]Rates calculated from equation (2) for experimental conditions using pure element sputter yields and assuming sputter-equilibrated surface
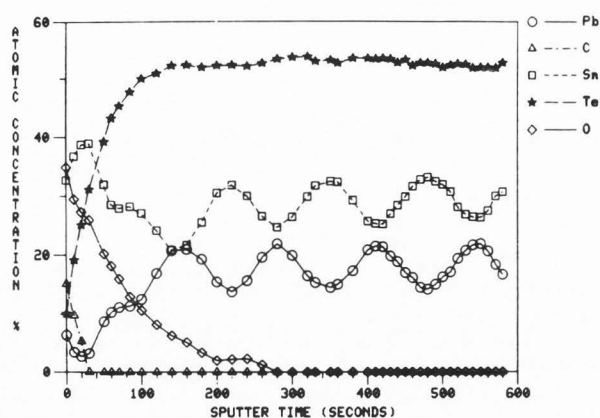
Figure 5. Depth profile of PbTe/SnTe superlattice film.

Returning to the question of the rounded corners, lowered maxima, and raised minima of the Pb and Sn profiles, the explanation may be inter-layer diffusion or artifacts of the analysis process (or some combination of the two). Among the artifacts that must be considered are (1) finite Auger analysis depth (escape depth effects), (2) preferential sputtering, and (3) sputter induced mixing of the layers.

The escape depth for Auger electrons (or more properly, the inelastic mean free path, IMFP) depends primarily on the energy of the electrons and to a lesser extent on the matrix. To a first approximation, the IMFP may be estimated from a "universal" expression that ignores matrix effects. Such an expression is available, developed from a compilation of experimental data (Seah and Dench, 1979). Values of the calculated IMFP for the Auger lines used here range from 0.5 to about 2 nm, well below the estimated individual layer thickness of 5 to 7 nm. The IMFP for the Pb Auger line is as low as 0.5 nm for pure lead to 1 nm for lead compounds; these low values suggest that there will be minimal distortion of the profile at the center of a 5 nm SnTe layer due to "looking ahead" to a PbTe layer below. The IMFP values for the Sn Auger line lie between 1 and 2 nm and imply a 10% or less effect at the center of a 5 nm PbTe layer. Thus, sampling depth effects can account for only a small part of the large distortion in the Pb and Sn profiles.

Sputtering effects are not as easily estimated. Preferential sputtering can be expected to occur whenever sputter rates differ significantly among the elements present. As we have seen, this is the case for Sn, Te and Pb. When the individual sputter rates are known, the bulk composition can be calculated from the measured equilibrium surface composition that is the result of preferential sputtering. But there are two problems: (1) results of such calculations seldom agree with the actual measured values, probably because of matrix effects, and (2) many monolayers must be removed

to reach equilibrium. The first problem means that any result must be treated as an estimate only. It is especially acute for superlattice films which change composition in relatively short distances. It has been estimated that tens of monolayers must be removed to achieve a sputter-equilibrated surface on a typical homogeneous sample. For the films analyzed, tens of monolayers is comparable to the layer thickness. Moreover, for the present case where the ideal square wave profile has been rounded (apparently by interdiffusion), the composition is changing continuously and equilibrium could not be established.

It is likely that the sputter equilibration process is changing the profile to some extent. On the other hand, sputter damage is known to anneal out very rapidly at room temperature for (Pb,Sn)Te (Buchner et al., 1979). That argues for equilibrium being reached in much shorter distances than for typical samples. The same argument suggests that interdiffusion of the two layers is the dominant effect.

Tribology: Effects of Additives in a Lubricated System

The scanning Auger microprobe can significantly aid in identifying the mechanisms which lower friction and reduce wear in ceramic-ceramic, ceramic-metal, and metal-metal systems. SEM and energy dispersive x-ray spectroscopy are often used to study morphology and chemical composition. However, the insensitivity to light elements (those lighter than Na) in most instruments and the relatively large depth of the analysis (on the order of 1 μm) limit the usefulness of these techniques. In contrast, Auger has excellent sensitivity for light elements and can examine the top few atom layers, where the tribological interactions occur and where the important reaction layers are formed. In addition, the ability to determine the chemical state of certain elements from the Auger spectra can give significant insights into the reactions taking place.

Auger analysis was used in the study of the friction behavior of four oils in tests of simulated cast iron camshafts (in the form of rings) running against sections of cast iron tappets (in the form of blocks) in a normal ambient atmosphere. The four fully formulated engine oils consisted of (1) a standard ASTM reference oil, (2) a friction-modified ASTM reference oil containing a soluble molybdenum additive, (3) a commercial friction-modified oil containing a second soluble molybdenum additive, and (4) a commercial friction-modified oil without molybdenum.

Friction measurements were made in a modified, commercial friction and wear test machine, in which line contact was made between ring and block and subjected to fully flooded lubrication with the oil maintained at a temperature of 100 $\pm$ 10 C. Specimens of both rings and blocks were examined by scanning Auger microscopy. The friction tests revealed differences in the performance of the oils that will be discussed below in reference to the Auger results.

Short sections of the rings were cut using a diamond wheel with isopropanol as a cutting fluid, and blocks were analyzed without cutting. All samples were cleaned in petroleum ether, followed by ethanol. Of course, it would have been preferable to avoid cleaning and the resultant changes in surface composition. However, the ultrahigh vacuum environment requires removal of high vapor pressure compounds. The cleaning procedure used is believed to cause minimal change in the relatively thick layer of the surface modified by the rubbing contact.

The layers produced on sliding surfaces in fully formulated oils are chemically very complex. They typically contain eight or more elements, sometimes in different chemical forms. Many of the elements are present at low levels, making quantitative measurements difficult. Moreover, the composition varies from point to point across the surface, as well as with depth. In our instrument, the spatial resolution was not sufficient to address the variation across the surface, and we employed a defocused beam to get an average of the various features. Depth profiles obtained are shown in Figure 6.

Despite the complexities and limitations, the data contained two especially notable features: (1) the presence of more phosphide and less phosphate for oil 2, containing high levels of molybdenum, and (2) a strong surface compositional asymmetry between the block and the ring for oil 4.

Although the presence of phosphate on the surface is expected, the presence of phosphide is not, given that the oils all contained the antiwear additive, zinc dialkyldithiophosphate (ZDP). Reduction of phosphate to phosphide is known to occur under conditions that exclude molecular oxygen from the contact zone (Willermet, et al., 1983), but those conditions do not apply here. The reduction is not thermodynamically favored in the presence of molecular oxygen. We believe the reduction is not an artifact due to electron beam effects; the electron beam current density was 0.3 mA/cm^2, low enough to avoid reduction, as we discussed above. The data suggest that the production of the phosphide is related to the presence of sufficient levels of soluble molybdenum additive, acting in some way as an oxygen scavenger in the contact zone.

The second feature, the compositional asymmetry for oil 4, consisted of a large excess of carbon over oxygen (a 3:1 ratio) for the ring and the reverse (a 1:3 ratio) for the block. It arose because of the contact kinematics existing in the friction test machine. The results from the test machine for oil 4 gave a high coefficient of friction (0.11), comparable to that for the reference oil 1 (0.10) and about double that for oils 2 and 3 (0.04 and 0.05, respectively). However, these friction results are not in accord with valve train torque measurements, which showed oil 4 to have a much lower torque than oil 1. The discrepancy can be understood by realizing that the contact kinematics of the test machine differ from those of an actual cam/tappet contact. In particular,

the block in the test machine is under constant load (and is never exposed to the oil directly), but in the cam/tappet system, the contact patch is continually moving relative to both cam and tappet surfaces. That is, the sliding surface of the rotating cam is contacting the rounded end of the tappet at a continuously changing angle and position, and the tappet is additionally free to rotate about its axis. Thus, the test machine geometry is inherently asymmetric, in contrast to the more nearly symmetric cam/tappet geometry. The Auger results reflect the asymmetry of the test machine geometry and suggest that the nature of the boundary layers obtained with oil 4 and the resulting friction values are sensitive to such contact kinematic effects.
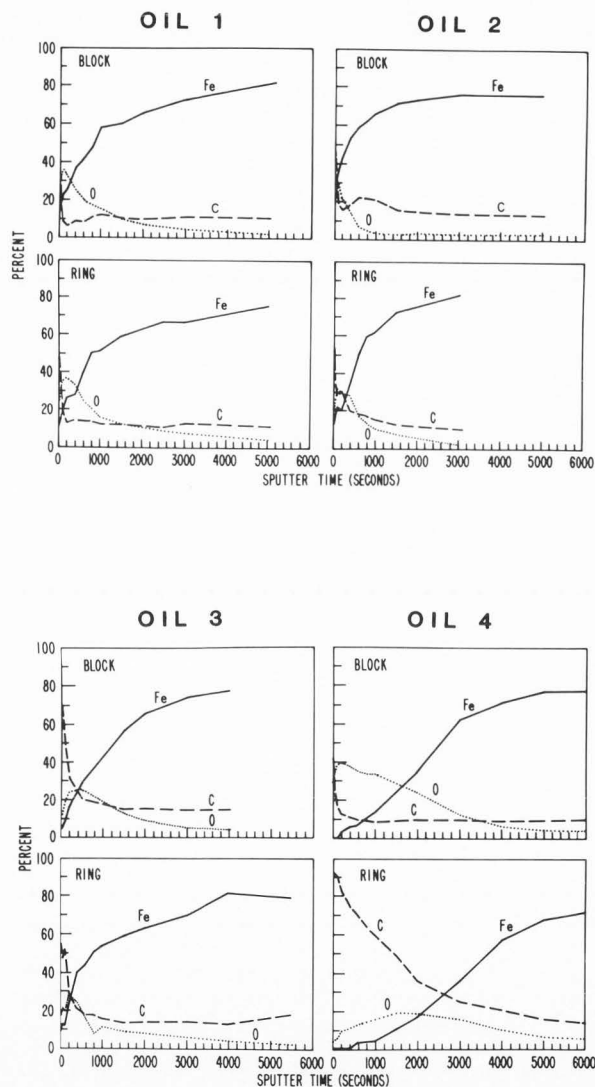

Figure 6. Depth profiles for four oils as a function of ring or block sample type.

Corrosion

Phosphate Conversion Coatings.

The use of phosphating to protect metal surfaces from corrosion has been well-known for over 50 years (Lorin, 1974). However, research has continued in an effort to develop new processes, optimize existing treatment operations and solve problems which arise in use. The basic phosphating process is to immerse the steel in, or spray onto the steel, a dilute phosphoric acid solution saturated with one or more metallic ions, such as zinc and iron. The result is a conversion of the metallic surface to an insoluble, crystalline, phosphate coating of the order of 10 μm in thickness which is integral with the surface and which can provide corrosion resistance. We became involved when one of the vendors to the Company was studying new methods of depositing phosphate coatings on certain automotive body steels. Samples representing early stages of growth showed large bare patches, thought to indicate potential coverage problems with the new formulation. Even though the surface appeared bare using optical microscopy and scanning electron microscopy with energy dispersive x-ray analysis, scanning Auger microscopy provided chemical information to show that the surface had, in fact, been treated.

In this case, the limited spatial resolution of the scanning Auger instrument (about 5 μm) did not allow the imaging and identification of "bare" and phosphated regions directly. However, we defocused the electron beam to a diameter of 240 μm to include areas of both types and then obtained a depth profile. We were able to conclude from the profile that (1) no bare steel was present, and (2) the "bare" areas consisted of a thin phosphate film having relatively high amounts of a proprietary additive which would act as suitable phosphate deposition sites if the process had continued for longer times. Samples which received longer depositions were subsequently examined and were shown to be fully covered with phosphate crystals.

Analysis of a Corrosion Layer on Stainless Steel Trim.

We were given the problem of trying to explain the occurrence of a dull (or cloudy) film on stainless steel bodyside molding trim from a test car. The trim could not be cleaned by normal washing procedures, but required cleaning using an abrasive material, a process which was potentially harmful to adjacent painted surfaces. The trim consisted of a bimetal combination of 434 ferritic stainless steel bonded to 3003 aluminum, with the stainless steel as the outer, visible surface. Aluminum was present to cathodically protect the cold rolled steel of the automobile body by acting as a sacrificial anode during galvanic corrosion from road salt (Beigay and Zaremski, 1972; Baboian, 1977; Redmerski, 1978).

Analysis of the exposed trim samples showed that the film was about 100 nm thick and contained regions rich in Ca, surrounding patches rich in Si; both areas were high in O, and contained smaller amounts of Al, Mg and Zn. Although insufficient carbon was seen in the Auger spectra to indicate the presence of the carbonate radical, we believe the calcium was present as $CaCO_3$. We have found that electron beam effects (and probably vacuum-induced changes, as well) cause the surface of freshly cleaved calcite crystals to be modified to calcium oxide, even when electron beams with very low current density are used. Spectra for the calcium rich regions on the trim and for calcite are similar. The calcium carbonate on the trim originated from dissolved minerals present in the surface water or from calcium chloride used for deicing. Silicon, as well as Mg and Al, are commonly found in the high silicate road dirt; Al could also have originated from the underside of the trim. The traces of Zn on the top surface of the film probably originated from galvanized vehicle components.

The presence of calcium carbonate is consistent with the design function of the stainless steel being cathodic to the underlying aluminum. But by being cathodic it is a favored site for carbonate deposition (Wolfson and Hartt, 1981; Butler and Ison, 1966). The presence of silica-rich patches can also be explained by galvanic corrosion. Silica is deposited at local anodic sites on the stainless steel when it loses electrical contact with the aluminum and the auto body steel (Speller, 1951). Such electrical isolation can happen when the moisture layer breaks into patches during evaporation. The result is tightly adhering patchy films, as observed.

Catalyst Research

Earlier work in our laboratory on oxidation of the Pt/Rh binary alloy system had shown surface enrichment of rhodium (Williamson et al., 1980). In the present study, Auger analysis was used to study oxidation and surface enrichment in Pd/Rh alloys (Joshi et al., 1986). Pure Pd, Pd/5% Rh and Pd/15% Rh alloy foils were heated for 4 hours in either an oxidizing atmosphere or in vacuum at temperatures between 600 and 1100 C. The resulting surfaces were analyzed, and the near surface region was characterized by depth profiling.

The Auger results showed the foil surface enriched in Pd as an oxide when heated in air to temperatures up to 800 C. Between 850 and 1100 C, Rh enrichment was observed at the surface with the amount decreasing with increasing temperature. The prevalence of palladium oxide at lower temperatures is not what one would predict from either the free energies of formation or from the temperatures at which PdO and Rh_2O_3 are known to dissociate (at about 870 and 1150 C, respectively). However, the observed drop in the Pd level and concurrent increase in Rh at about 850 C is likely related to PdO being unstable at these temperatures. Similarly, the disappearance of a substantial oxide layer and the reversion of the surface to a bulk-like composition above about 1000 C is likely a consequence of both oxides having exceeded their stability limits.

An interesting sidelight to the study was the observation of a thin silicon dioxide layer on samples heated in air to $\geq$900 C and a thick layer (a few tens of nanometers) on all samples heated in a high vacuum environment. Such

segregation of Si, which exists as an impurity (<10 ppm) in the bulk, was also observed on samples heated in ultrahigh vacuum (Graham et al., 1986).

An unusual artifact observed during analysis was the reduction of the palladium oxide when the surface was maintained at ultrahigh vacuum for extended periods (>10 hours). During a typical spectrum acquisition time, the reduction was found to be negligible. But interruption of a depth profile overnight caused a significant difference in surface composition.

The question of preferential sputtering was taken up by another group of workers at Ford, who made a more detailed study of the Pd/15% Rh alloy, confirming the surface enrichments as described above and extending the study to include the effects of time at temperature (Graham et al., 1986). They found evidence for the preferential sputtering of Pd with respect to Rh and showed that the presence of oxygen tended to reduce preferential sputtering.

Conclusion

Auger electron spectroscopy has a great many industrial applications. As we have seen in this presentation, problems can be as technologically relevant as bonding galvanized steel sheet or developing new catalyst materials. For an industrial research facility, more esoteric problems can arise, such as trying to develop an understanding of complex sputtering phenomena.

In nearly all cases, there are unexpected complexities which make what looks initially like a simple analysis to be something more difficult. Electron and ion beam interactions with the surface usually cause problems and make the data difficult to interpret quantitatively. In the case of electron beams, charging effects and beam reduction frequently occur when dealing with non-conducting materials. Ion beam effects occur whenever sputtering is used, which it is for nearly all analyses. Such effects as preferential sputtering, ion beam reduction, and sputter-induced mixing at interfaces can often be minimized (for example, by choosing lower ion energies), but they must be considered when interpreting the data. Even variations in sputter rate from material to material can cause problems. Often standards of the same composition as the sample and with known thickness are not available for determining sputter rates. Considerable error can result if rates from such common standards as Ta_2O_5 and SiO_2 are used as the direct estimate for other materials. Our example of the PbTe/SnTe superlattice characterization shows that rates may be as much as an order of magnitude different from that of Ta_2O_5.

Sample effects are also important. Surface roughness must be taken into account in interpreting both surface spectra and depth profiles. In that regard, high spatial resolution in scanning Auger analysis is crucial for sample characterization. Even if the Auger analysis area must be larger than the minimum electron beam size (as is often the case for signal to noise considerations), having sufficient spatial resolution to reveal surface structure at the point of analysis is an important capability. Sample preparation and mounting present obstacles. Many of the samples which we are called upon to analyze are not of optimal shape. Powders are difficult to mount and can compromise the vacuum environment unless they are sufficiently outgassed before analysis. Bulky objects such as windshields or automobile body parts have to be carefully sectioned into suitable samples. And there is always the ever-pervasive influence of contamination: everyone seems to want to touch the areas of interest.

We have seen the use of Auger grow continuously. Obviously, we have been able to touch on only a limited number of applications in this paper; there are many more. Perhaps 50 new materials and components are annually being brought to our laboratory to use scanning Auger microscopy as a means of solving a problem. Ford's Glass Division has come to rely on surface analytical information as it develops technologically advanced coatings for glass in vehicle and architectural applications. The vehicle is becoming more and more an electrical maze of switches, sensors, and integrated circuits, all of which seem to exhibit surface-related problems during development. The future is obviously exciting, and continuing growth in scanning Auger microscopy is assured.

Acknowledgements

References

1. Baboian R. (1977). Corrosion behavior of trim materials on automobiles. SAE Paper 770110, pp 1-9.

2. Beigay JM, Zaremski DR. (1972). Aluminum striped stainless trim for prevention of auto body galvanic corrosion. SAE Paper 720515, pp 1-9.

3. Bevolo AJ. (1981) Results of a Ta_2O_5 sputter yield round robin. Surf. Interface Anal. 3, 240-242.

4. Briggs D, Seah MP. (1983). Practical Surface Analysis. John Wiley & Sons Limited, London, p 1.

5. Bucci GD. (1984). New copper foils for printed circuit boards. IPC Technical Paper IPC-TP-501, pp 1-16.

6. Buchner S, Sun TS, Beck WA, Byer NE, Chen JM. (1979). Schottky barrier formation on (Pb,Sn)Te. J. Vac. Sci. Technol. 16, 1171-1173.

7. Butler G, Ison HCK. (1966). Corrosion and its Prevention in Waters. Reinhold Publishing Corp., New York, p. 16.

8. Casper LA, Powell CA. (1982). Industrial Applications of Surface Analysis. American Chemical Society, Washington, DC, p 1.

9. Davis LE, MacDonald NC, Palmberg PW, Riach GE, Weber RE. (1976). Handbook of Auger Electron Spectroscopy. Second Edition. Physical Electronics Div., Perkin-Elmer Corp., Eden Prairie, MN, pp 1-18.

10. Feldman LC, Mayer JW. (1986). Fundamentals of Surface and Thin Film Analysis. Elsevier, New York, p 1.

11. Graham GW, Potter T, Baird RJ, Gandhi HS, Shelef M. (1986). Surface composition of polycrystalline Pd15Rh following high temperature oxidation in air. J. Vac. Sci. Technol. A 4, 1613-1616.

12. Gray DE, Editor. (1972). American Institute of Physics Handbook, 3rd Edn. McGraw-Hill Book Co., New York, p. 9-22.

13. Holloway H. (1980). Thin-film IV-VI semiconductor photodiodes. In Physics of Thin Films, Vol. 11. Academic Press, Inc., New York, pp 105-203.

14. Joshi BM, Gandhi HS, Shelef M. (1986). Surface enrichment of rhodium in Pd-Rh alloys after high temperature air oxidation. Surf. Coat. Techn. 29, 131-140.

15. Lorin G. (1974). Phosphating of Metals. Finishing Publications Ltd., Hampton Hill, Middlesex, UK, pp 1-23.

16. Redmerski LS. (1978). Corrosion behavior in automotive trim applications. in Design for Automotive Corrosion Protection, SAE Proceedings P-78, Paper 780917, pp 750-755.

17. Seah MP. (1981). Pure element sputtering yields using 500-1000 eV argon ions. Thin Solid Films 81, 279-287.

18. Seah MP, Dench WA. (1979). Quantitative electron spectroscopy of surfaces. Surf. Inter. Anal. 1, 2-11.

19. Speller FN. (1951). Corrosion. Causes and Prevention. 3rd Edn. McGraw-Hill Book Co., Inc., New York, p. 390.

20. Thompson M, Baker MD, Christie A, Tyson JF. (1985). Auger Electron Spectroscopy. John Wiley & Sons, New York, p. 1.

21. van Ooij WJ. (1977). Surface composition, oxidation and sulfidation of cold-worked brass and brass-coated steel wire as studied by x-ray photoelectron spectroscopy. Surf. Techn. 6, 1-18.

22. Willermet PA, Kandah SK, Siegl WO, Chase RE. (1983). The influence of molecular oxygen on wear protection by surface active compounds. ASLE Trans., 26, 523-531.

23. Williamson WB, Gandhi HS, Wynblatt P, Truex TJ, Ku RC. (1980). Surface segregation and effects on selective chemical reactions over platinum-rhodium three-way catalysts. AIChE Symp. Ser., No. 201, 76, 212-223.

24. Wolfson SL, Hartt WH. (1981). An initial investigation of calcerous deposits upon cathodic steel surfaces in sea water. Corrosion 37, 70-76.

Discussion with Reviewers

<u>S.A. Files</u>: In reference to the printed circuit foil, what is meant by protection from "staining' and what is a conversion layer?
<u>Authors</u>: The conversion layer referred to is a corrosion-inhibiting coating applied from a bath containing hexavalent chromium. The layer formed is fairly complex, incorporating oxides and chromates of the basis metal itself, hence the term "conversion." Its use prevents the growth of thick oxide layers and other products of reaction with the ambient (referred to in the industry as "staining") that might affect the adhesion of the foil to the epoxy board.

<u>S.A. Files</u>: In the friction additive study, is it possible that the reduction of phosphate to phosphide could be due to sample preparation or differences in sample response to the vacuum environment and ion (sputter and analysis) beam effects?
<u>Authors</u>: We feel that sample preparation had little effect on phosphate reduction, given that all samples were prepared identically and that differences were observed between them. Concerning ion beam effects on reduction of phosphate, we found in the study of IC facility tubing contamination that sputtering for more than 1000 seconds caused no noticeable reduction of a very strong phosphate signal. We feel that ion beam effects under the conditions we used were negligible. Exposure of phosphate surfaces to the vacuum environment has no measurable effect in our experience. While phosphate is known to suffer reduction by sufficiently high electron beam doses, it is not among the most sensitive of compounds. We point out, for example, that calcium carbonate is so sensitive that we have trouble seeing any carbon in its spectrum under the mildest of conditions, and there are indications that the vacuum environment may alter the surface composition.

<u>S. A. Files</u>: Have any comparisons to ESCA analysis for phosphate/phosphide been made, especially with regard to quantitative analysis?
<u>Authors</u>: We have done no x-ray photoelectron spectroscopy of phosphate compounds. However, both AES and XPS spectra are reported for phosphate and phosphide by Bernett et al. [Bernett MK, Murday JS, Turner NH. (1977). An interpretation of the Auger LVV transitions from oxides of third-row elements. J. Elec. Spectros. Rel. Phen. 12, 375-393].

<u>H. Hantsche</u>: In your expression (2) for the sputter rate of compounds it is assumed, that there is a linear relationship between the elemental sputter yield and the concentration of the element, which surely is the easiest assumption. How far could that be from reality?
<u>Authors</u>: The basic assumptions made in deriving equation (2) were twofold: (a) the sputter **rate** of each element is proportional to the <u>surface</u> concentration (assumed different from the bulk) times the sputter **yield** for the element and (b) at steady state the sputter rate for each element is proportional to the <u>bulk</u> concentration of that element. Such assumptions should be very close to reality, with the caveat that steady state might not have been reached. (See the discussion on this point near the end of the section in question.) As also mentioned in that section, the use of pure element sputter yields was the least justified assumption because the matrix

affects sputter yields.

S.W. Gaarenstroom: The authors use very long sputter-depth profile times, to minimize some ion beam-induced effects. Could they comment on instrument stability during these long data acquisition times? (Auger energy shifts, sputter rate drift, specimen movement)

Authors: It is certainly true that instrument stability issues are involved in the trade-off with ion beam effects. On the other hand, we observed no significant shifts of Auger energies with time. We point out that depth profiles were obtained using an alternating mode, in which sputtering was suspended while partial or full spectra were acquired. Small shifts of Auger energies can be important if data are acquired automatically and composition is determined using a two or three point scheme where the energy corresponding to the peak must be set initially. Specimen movement was not critical, given the large electron beam diameter and low image magnifications used for most studies. It is a much more critical issue when high spatial resolution is involved; in those cases, the specimen position must be "steered" by monitoring the image location during long sputter times to keep the analysis points invariant. Sputter rate drift is potentially the most serious problem. It was our experience that ion gun parameters remained stable, but we did not monitor ion beam current directly. Internal evidence that large changes did not occur can be found in profiles such as that in Figure 5, where the periodicity remained constant as a function of time.

S. Thomas: Please define resolution for the SAM versus the SEM.

Authors: The spatial resolution (electron beam diameter) of a modern SAM can be as good as 25 nm in the imaging mode, contrasted with 200 nm or 3 μm for older SAM's and compared with 5 nm for a typical SEM. While imaging is largely determined by the electron beam size, Auger electrons used for elemental mapping and line scans originate in a somewhat larger region. Backscattered electrons from the subsurface region create Auger electrons in a halo around the electron beam spot to cause this degradation of spatial resolution and set a lower limit of about 100 nm on localization of elemental information.

S. Thomas; Concerning sample handling, the ASTM E-42 committee has a "recommended practice." Please comment.

Authors: ASTM Standard E1078-85 deals with a wide range of specimen handling issues pertaining to surface analysis. Our use of sectioning techniques and solvents conforms with recommended practice.

S. Thomas: The authors state that their sputtering conditions minimized sputtering artifacts. How?

Authors: Ion beam damage to the surface increases with ion energy, as does sputter rate over the range of energies (0-5 keV) available on our ion gun. The choice of 2 keV represents a compromise between total sputter time and induced damage.

S. Thomas: The authors state that it is common practice to assume that the sputter rate for the sample of interest is not too different from that for Ta_2O_5. Who does this? Why?

Authors: A reading of the literature will produce many examples in which the sputter rate is quoted as that for Ta_2O_5 without further comment or with the implication that it is applicable to the material analyzed. Although there are probably a number of reasons why it is done, lack of sputter rate data or standards for layers that are compositionally complex is an important one. While reporting the sputter rate of Ta_2O_5 is a useful measure of the ion beam conditions, it does not adequately characterize the sputter rate of the material analyzed and can be grossly misleading. One reason for detailing the example of PbSnTe was to point out that danger.